A bridge between the single-photon and squeezed-vacuum states

Nitin Jain[1,2], **S. R. Huisman**[1,3], **Erwan Bimbard**[1,4], **and A. I. Lvovsky**[1,*]

[1]*Institute for Quantum Information Science, University of Calgary, Calgary, Alberta T2N 1N4, Canada*

[2]*Max Planck Institute for the Science of Light, Günther-Scharowsky-Str. 1, 91058 Erlangen, Germany*

[3]*Complex Photonic Systems (COPS), Faculty of Science and Technology and MESA+ Institute for Nanotechnology, University of Twente, 7500 AE Enschede, The Netherlands*

[4]*Department of Physics, Ecole Normale Supérieure, 24 rue Lhomond, 75005 Paris, France*

[*]*LVOV@ucalgary.ca*

Abstract: The two modes of the Einstein-Podolsky-Rosen quadrature entangled state generated by parametric down-conversion interfere on a beam splitter of variable splitting ratio. Detection of a photon in one of the beam splitter output channels heralds preparation of a signal state in the other, which is characterized using homodyne tomography. By controlling the beam splitting ratio, the signal state can be chosen anywhere between the single-photon and squeezed state.

OCIS codes: (270.6570) Squeezed states; (270.5290) Photon statistics; (270.5585) Quantum information and processing

References and links

1. Quantum Information with Continuous Variables of Atoms and Light, N. Cerf, G. Leuchs, and E. Polzik (Eds.), World Scientific, Singapore, 2007
2. P. Kok, W. J. Munro, K. Nemoto, T. C. Ralph, J. P. Dowling, and G. J. Milburn, "Linear optical quantum computing with photonic qubits", Rev. Mod. Phys. **79**, 135–174 (2007)
3. A. I. Lvovsky, H. Hansen, T. Aichele, O. Benson, J. Mlynek and S. Schiller, "Quantum State Reconstruction of the Single-Photon Fock State", Phys. Rev. Lett. **87**, 050402 (2001)
4. A. Zavatta, S. Viciani, and M. Bellini, "Tomographic reconstruction of the single-photon Fock state by high-frequency homodyne detection", Phys. Rev. A **70**, 053821 (2004)
5. S. R. Huisman, N. Jain, S. A. Babichev, F. Vewinger, A. N. Zhang, S. H. Youn, A. I. Lvovsky, "Instant single-photon Fock state tomography", Opt. Lett. **34**, 2739-2741 (2009);
6. A. Zavatta, S. Viciani, and M. Bellini, "Quantum-to-Classical Transition with Single-Photon-Added Coherent States of Light", Science **306**, 660–662 (2004).
7. A. Ourjoumtsev, R. Tualle-Brouri, J. Laurat, and P. Grangier, "Generating Optical Schrdinger Kittens for Quantum Information Processing", Science **312**, 83–86 (2006).
8. G. Puentes, J. S. Lundeen, M. P. A. Branderhorst, H. B. Coldenstrodt-Ronge, B. J. Smith, and I. A. Walmsley, "Bridging Particle and Wave Sensitivity in a Configurable Detector of Positive Operator-Valued Measures", Phys. Rev. Lett. **102**, 080404 (2009)
9. E. Bimbard, N. Jain, A. MacRae and A. I. Lvovsky, "Quantum-optical state engineering up to the two-photon level", Nature Phot. **4**, 243–247 (2010)
10. H. Takahashi, J. S. Neergaard-Nielsen, M. Takeuchi, M. Takeoka, K. Hayasaka, A. Furusawa, and M. Sasaki, "Entanglement distillation from Gaussian input states", Nature Phot. 4, 178–181 (2010)
11. U. Leonhardt, *Measuring the quantum state of light* (Cambridge University Press, Cambridge, 1997)
12. A. I. Lvovsky and M. G. Raymer, "Continuous-variable optical quantum-state tomography", Rev. Mod. Phys. **81**, 299–332 (2009).

#128873 - $15.00 USD Received 4 Jun 2010; revised 2 Jul 2010; accepted 5 Jul 2010; published 10 Aug 2010

13. T. Aichele, A. I. Lvovsky, S. Schiller, "Optical mode characterization of single photons prepared via conditional measurements on a biphoton state", Eur. Phys. J. D **18**, 237–245 (2002)
14. A. I. Lvovsky, "Iterative maximum-likelihood reconstruction in quantum homodyne tomography", J. Opt. B: Q. Semiclass. Opt. **6**, S556–S559 (2004).
15. J. Řeháček, Z. Hradil, E. Knill and A. I. Lvovsky, "Diluted maximum-likelihood algorithm for quantum tomography, Phys. Rev. A **75**, 042108 (2007).
16. J. Appel, D. Hoffman, E. Figueroa and A. I. Lvovsky, "Electronic noise in optical homodyne tomography", Phys. Rev. A **75**, 035802 (2007)
17. W. Wasilewski, A. I. Lvovsky, K. Banaszek and C. Radzewicz, "Pulsed squeezed light: simultaneous squeezing of multiple modes", Phys. Rev. A 73, 063819 (2006)
18. A. I. Lvovsky, W. Wasilewski and K. Banaszek, "Decomposing a pulsed optical parametric amplifier into independent squeezers", J. Mod. Opt. 54, 721–733 (2007)
19. Y. Bar-Shalom and X.-R. Li, *Estimation with Applications to Tracking and Navigation (John Wiley & Sons, New York, 2001)*
20. *L. Mandel and E. Wolf,* Optical Coherence and Quantum Optics *(Cambridge University Press, New York, 1995)*

1. Introduction

Nonclassical states of light present an important tool in testing fundamental quantum physics and quantum information processing. Among the most basic quantum optical states are the squeezed-vacuum states that exhibit reduced quadrature noise at certain phases, and the photon number states (Fock states) with a well-defined energy. The former were among the first nonclassical states of light to be generated experimentally and are the basis for a variety of continuous-variable quantum information protocols [1]. Such states feature positive Gaussian Wigner functions and their field quadrature noise is strongly phase dependent. Fock states, especially the single-photon state, are natural candidates for encoding quantum information in the discrete-variable representation (qubits) [2]. Their Wigner functions show non-Gaussian characterisitics such as oscillations and negativities and are phase-independent [3, 4, 5].

These "discrete-variable" and "continuous-variable" pillars of quantum-optical technology developed separately for a long time, each associated with its own set of production and detection methods as well as applications. Recently, these pillars have been bridged by a variety of experiments extending the range of the Hilbert space accessible to quantum technology beyond the framework of either domain [6, 7, 8, 9, 10].

In this paper we report an experiment that demonstrates the connection between the discrete and continuous domains of quantum optics very explicitly. We start with a two-mode squeezed vacuum state produced through parametric down-conversion in a spectrally and spatially degenerate, but polarization-nondegenerate configuration. The two modes of this state are overlapped on a beam splitter of variable splitting ratio, formed by a half-wave plate (HWP) and a polarizing beam splitter (Fig. 1). One of the output channels of the beam splitter (*trigger*) is subjected to a measurement by a single-photon detector. Conditioned on a photon-detection event, and dependent on the reflectivity of the beam splitter, a particular quantum state of light in the other channel (*signal*) is prepared.

We write the two-mode state produced by down-conversion in the photon number basis as

$$|\Psi\rangle = \sqrt{1-\gamma^2}\left[|0_s,0_i\rangle + \gamma|1_s,1_i\rangle + O(\gamma^2)\right], \tag{1}$$

where the signal and idler modes are represented by s and i, respectively, and γ is the down-conversion amplitude, which is assumed small. If the beam splitter reflectivity R equals 0 or 1, the two-mode squeezed state remains unaltered. With a small γ (as is the case in our experiment), a "click" of the single-photon detector heralds the preparation of the single photon in the signal channel with a high probability. On the other hand, a beam splitter with a reflectivity of $1/2$ converts the two-mode squeezed vacuum into a tensor product of two single-mode squeezed-vacuum states [11]. To elaborate in the photon number basis, the first order term in

#128873 - $15.00 USD Received 4 Jun 2010; revised 2 Jul 2010; accepted 5 Jul 2010; published 10 Aug 2010

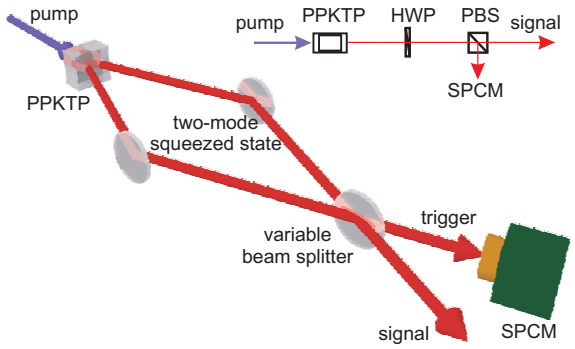

Fig. 1. Concept of the experimental setup. The figure is for illustration purpose only; the inset shows the actual implementation of parametric down-conversion and the variable beam splitter. HWP, half-wave plate; PBS, polarizing beam splitter; SPCM, single-photon counting module. The down-conversion is spatially and spectrally-degenerate, but polarization-nondegenerate.

Eq. (1) undergoes a Hong-Ou-Mandel type transformation $|1_s,1_i\rangle \rightarrow \frac{1}{\sqrt{2}}(|2_s,0_i\rangle - |0_s,2_i\rangle)$, so the beam splitter output state can be approximated as

$$|\Psi\rangle_{\text{out}} \approx \sqrt{(1-\gamma^2)}\left[|0_s\rangle + \frac{\gamma}{\sqrt{2}}|2_s\rangle\right]\left[|0_i\rangle - \frac{\gamma}{\sqrt{2}}|2_i\rangle\right]. \tag{2}$$

Independent of the measurement result in the trigger channel, the signal state is then squeezed vacuum. In this way, by simply rotating the waveplate that determines the beam splitter reflectivity, we can choose the output to be the squeezed-vacuum or single-photon state, or anything in between.

2. Experiment

The operation of the setup is explained in detail in Ref. [5]; a brief description relevant to this article follows. A mode-locked Ti:Sapphire laser (Coherent MIRA 900) emits transform-limited pulses of width around 1.7 ps and a repetition rate of about 76 MHz. The laser output, centered at a wavelength ~790 nm, is frequency doubled and focussed into a periodically-poled potassium titanyl phosphate (PPKTP) crystal, which is phase-matched for type II collinear down conversion. The two collinear output channels are mixed on the variable beam splitter (Fig. 1, inset), producing the trigger and signal modes. The trigger mode is subjected to spectral selection using a 0.3-nm bandwidth interference filter and spatial filtering with a single-mode optical fiber followed by measurement with a single photon counting module (Perkin-Elmer SPCM-AQR-14-FC).

The state in the signal mode, heralded by the detection event in the trigger channel, is characterized using optical homodyne tomography [12]. The local oscillator for homodyne detection is obtained from the master laser output. The spatio-temporal mode of the local oscillator pulses were matched to the signal state as described by Aichele *et al.* [13]. The difference photocurrent signal from the homodyne detector is amplified and digitized by an acquisition card (Agilent Acqiris DP211) that is triggered by the output of the SPCM. For each position of the HWP, a set containing 10^6 quadrature samples of the signal state plus 8×10^6 samples from 8 neighbouring pulses, is acquired. The signal channel is then blocked and a set containing 9×10^6

#128873 - $15.00 USD Received 4 Jun 2010; revised 2 Jul 2010; accepted 5 Jul 2010; published 10 Aug 2010

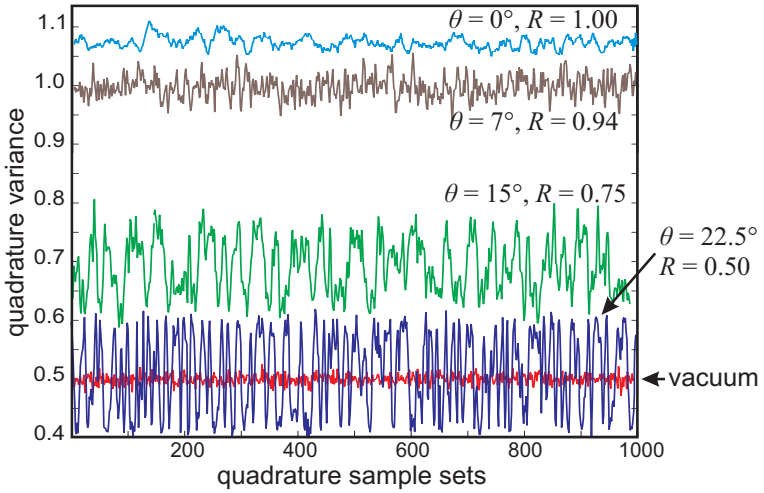

Fig. 2. Quadrature noise of the experimentally observed vacuum and signal states at different reflectivities of the variable beam splitter, for varying local oscillator phase. The angle θ of the half-wave plate and the corresponding beam splitter reflectivity (given by $R = \cos^2 2\theta$) are indicated for each curve. The observed quadrature noise is influenced by preparation and detection inefficiencies.

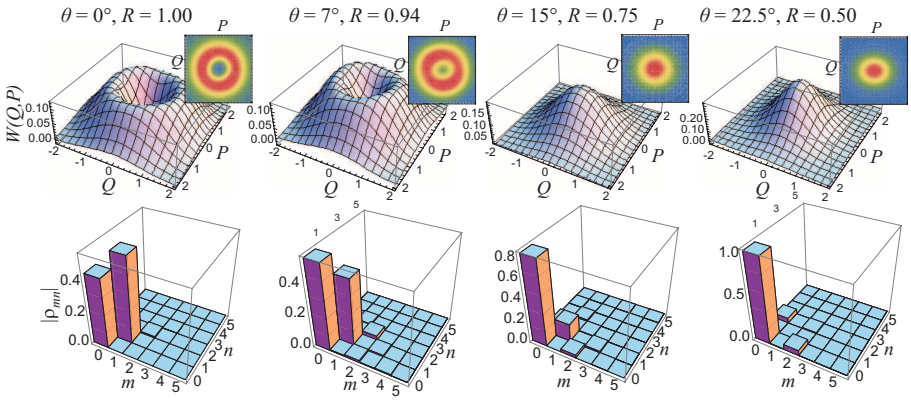

Fig. 3. Experimentally reconstructed Wigner functions (top row) and density matrices (absolute values, bottom row). The insets show contour diagrams associated to specific Wigner functions.

#128873 - $15.00 USD Received 4 Jun 2010; revised 2 Jul 2010; accepted 5 Jul 2010; published 10 Aug 2010

uniform vacuum state samples is acquired in order to calibrate the quadrature scale, assuming convention $\Delta Q^2 = 1/2$ for the vacuum state.

Figure 2 shows the experimentally measured quadrature variance ΔQ_ϕ^2 for the vacuum and signal states, acquired at four different HWP angles θ varying from 0 to 22.5°, corresponding to the beam splitter reflectivity $R = \cos^2 2\theta$ varying from 1 to $1/2$. Each point of the curves displayed is calculated from a set of 1000 quadrature samples, acquired within a time interval of ~ 0.02 s, during which the local oscillator phase does not change significantly.

The quadrature variance as a function of the local oscillator phase ϕ behaves as $\Delta Q_\phi^2 = A + B\cos 2\phi$ (in the extreme case of $\theta = 0^\circ$ one has $B = 0$). We utilize this dependence to determine the local oscillator phase for each set of 1000 quadrature samples: we first find the quantities A and B as, respectively, the median and amplitude of the quadrature variance, and then use inverse cosine to determine ϕ for each set. In this way, for each position of the wave plate except $\theta = 0$, we obtain 10^6 quadrature-phase pairs associated with the signal state. We then reconstruct the state using a quantum likelihood-maximization algorithm [14, 15], without correcting for any detection inefficiency. For $\theta = 0$, we assume random phase and determine only the diagonal elements of the density matrix in the Fock basis.

Figure 3 presents the density matrices and corresponding Wigner functions reconstructed from the experimentally retrieved data. One can observe a gradual transition from the single-photon to the squeezed-vacuum state. For the $\theta = 22.5^\circ$ ($R = 0.5$) case, the observed density matrix approximates that of a superposition of the vacuum and two-photon states, and the corresponding Wigner function exhibits squeezing of the momentum quadrature. On the other hand, for $\theta = 0^\circ$ ($R = 1$) the only significant density matrix elements are the diagonal elements corresponding to the single-photon and vacuum states, with a small admixture of the two-photon state. The vacuum component emerges due to linear losses, dark counts of the single-photon detector, mode mismatch between the signal and the local oscillator [13] and electronic noise of the homodyne detector [16], whose combined effect can be modeled by a non-unitary detection efficiency η [3]. From the density matrix, we obtain $\eta = 0.55$. The two-photon component appears because the SPCM is not a number-resolving detector, and can also "click" in response to the multiphoton terms in the down-conversion output. The fraction of such events scales as γ^2, which explains why the two-photon component has not been significant in similar measurements made in Refs. [3, 4] (where γ was very small), but is seen in the present experiment.

The extreme cases of $R = 0.5$ and $R = 1$ are further elaborated in Fig. 4. Part (a) of the figure shows a cross-section of the Wigner function of the single-photon state featuring negative values around the phase-space origin that are characteristic of this state. In Fig. 4(b), the variance of the quadrature noise as a function of the phase is displayed for the squeezed vacuum, showing a reduction of 0.62 dB below the standard quantum limit.

Gradual transition between the single-photon and squeezed-vacuum states is illustrated in Fig. 5. The maximum $\Delta Q_{\max}^2$ and minimum $\Delta Q_{\min}^2$ quadrature variances are shown in (a) as a function of the HWP angle. The behavior of the ratio $\Delta Q_{\max}^2/\Delta Q_{\min}^2$ is largely determined by the value of γ, and the best fit is obtained with $\gamma^2 = 0.025 \pm 0.002$, which is similar to the result $\gamma^2 = 0.016$ measured in Ref. [5] with the same setup, but in a different experimental run. In calculating the fit, we assumed a constant detection efficiency $\eta = 0.55$. The observed variances are generally consistent with the theoretical prediction. The discrepancies at intermediate angles can be attributed to errors in estimating the local oscillator phase as well as the complicated character of the spatiotemporal mode of the biphoton generated in a practical down-conversion setting [17, 18].

The behavior of the Mandel parameter $Q = \langle \Delta n^2 \rangle / \langle n \rangle - 1$ (where n is the photon number and $\langle \Delta n^2 \rangle$ the variance therof) of the signal state is displayed in Fig. 5(b). For $R = 1$ (the single-photon limit), the Mandel parameter is negative, manifesting the antibunched character

#128873 - $15.00 USD Received 4 Jun 2010; revised 2 Jul 2010; accepted 5 Jul 2010; published 10 Aug 2010

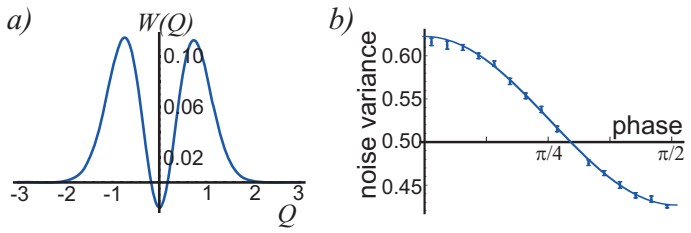

Fig. 4. Cross-section of the Wigner Function of the single-photon state (a) and the quadrature noise of the squeezed state as a function of the optical phase (b), obtained from their respective density matrices, experimentally reconstructed without correcting for detection inefficiency. The squeezing variance features a solid curve obtained from maximum-likelihood reconstruction, while the points with error-bars from 0 to $\pi/2$ are representative of the binned raw quadrature data. The error bars correspond to $\sigma_i\sqrt{2/N_i}$, σ_i being the width of a Gaussian distribution from N_i samples in each bin [19].

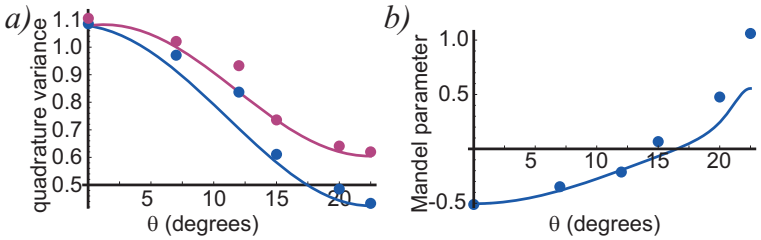

Fig. 5. Maximum and minimum variances of the measured quadratures (a) and the Mandel parameter of the reconstructed states (b) as functions of the HWP angle. The theoretical predictions are calculated for $\eta = 0.55$, $\gamma^2 = 0.025$ in the limit of low single-photon detection efficiency. The states with the minimum quadrature variance below $1/2$ or with a negative Mandel parameter are nonclassical.

of the signal state. The squeezed-vacuum limit, on the contrary, exhibits photon bunching. The discrepancy between the theory and experiment in this limit is explained by a low value of the denominator $\langle n \rangle$ that makes the experimental Mandel parameter susceptible to errors. Figs. 5(a) and (b) show complementarity of the two criteria of a quantum optical state's nonclassical character [20]: quadrature squeezing appears and photon antibunching disappears at about the same θ.

3. Summary

By mixing the output modes of a parametric down-converter on a variable beam splitter and detecting single photons in one of the beam splitter output channels, we prepared a variety of quantum states ranging from the single-photon Fock state to the squeezed-vacuum state in the other output channel. This experiment explicitly demonstrates that the discrete-variable and continuous-variable domains of quantum optics can be connected through a continuous set of states.

Acknowledgements

This work was supported by NSERC, CIAR, AIF, CFI and Quantum*Works*. We thank M. Lobino and K. Banaszek for helpful discussions.

#128873 - $15.00 USD Received 4 Jun 2010; revised 2 Jul 2010; accepted 5 Jul 2010; published 10 Aug 2010